THE ASTROPHYSICAL JOURNAL, 232:451–466, 1979 September 1

THE H II REGION–MOLECULAR CLOUD COMPLEX W51

STUART L. MUFSON
Indiana University, Bloomington
AND
HARVEY S. LISZT
National Radio Astronomy Observatory, Green Bank, West Virginia
Received 1978 September 18; accepted 1979 March 19

ABSTRACT

We have made new observations of the H II region–molecular cloud complex W51 in the spectral lines of $\lambda = 2.6$ mm CO, $\lambda = 3.1$ mm CS, $\lambda = 2$ cm H_2CO, and the recombination line H76α. Since the line of sight to this H II region lies nearly tangent to the Sagittarius spiral arm, W51 offers an excellent opportunity to study the activity associated with the large-scale spiral structure of our Galaxy. Our molecular observations are most consistent with a picture in which three streams of cold gas flow through the complex. These streams have been placed within the structure of the hydrogen observed in this neighborhood of the galactic plane. This study shows that the H II regions are now near the outside of these molecular streams, ionizing cold gas that flows into the low-pressure regions between the clouds. Simple models of the H II regions in the W51 complex have been constructed which reproduce many of the continuum and spectral line observations that have been obtained.

Subject headings: interstellar: molecules — nebulae: individual — radio sources: lines

I. INTRODUCTION

The radio source W51 was first reported by Westerhout (1958) in his $\lambda = 22$ cm survey of the galactic plane. Since that work, studies of the ionized gas in continuum and recombination line emission (Goss and Shaver 1970; Wilson *et al.* 1970) have revealed an unusually high degree of kinematic and morphological complexity in the W51 region. The further detection of molecular line features by Zuckerman *et al.* (1970) and Penzias, Jefferts, and Wilson (1971) demonstrated that the H II regions in this source are only part of an interacting system consisting of clouds of both ionized and dense neutral material.

Giant H II region–molecular cloud complexes like W51 and W49 A (Mufson and Liszt 1977, hereafter Paper I) are regions of recent star formation in our Galaxy. Because the line of sight to W51 lies nearly tangent to the Sagittarius spiral arm (Shane and Bieger-Smith 1966), the observed structure can be attributed to the unusually long path length over which bursts of star formation have occurred in this direction. In fact, were our Galaxy to be observed in Hα from a distance, the H II regions of the W51 complex would likely outline the Sagittarius spiral arm much as giant H II regions delineate the spiral arms of NGC 628 (Morgan and Osterbrock 1969). Consequently, W51 offers an excellent opportunity to study the activity associated with the large-scale spiral structure of our Galaxy.

The W51 continuum complex has been separated into four main components (Kundu and Velusamy 1967; Wilson *et al.* 1970) as shown in Figure 1: W51 A, comprising the sources G49.5−0.4 and G49.4−0.3; W51 B, consisting of G48.9−0.3, G49.0−0.3, G49.1−0.4, and G49.2−0.3; W51 C, or the eastern arm (Terzian and Balick 1969); and G48.6+0.0, a source whose H109α recombination line velocity places it away from the complex. Neutral atomic gas in the W51 complex has been studied by Burton (1966, 1970*a*, *b*), Burton and Shane (1970), and Radhakrishnan *et al.* (1972); the observations of OH have been discussed by Weaver, Dieter, and Williams (1968) and Slysh (1974). The distribution of H_2CO within the gas has been studied by Scoville and Solomon (1973), Fomalont and Weliachew (1973), and Bieging (1975); observations of carbon monoxide emission are given by Liszt (1973) and Scoville and Solomon (1973); carbon monosulfide emission has been reported by Turner *et al.* (1973) and Liszt and Linke (1975). Although optical emission from W51 was thought to be completely obscured by intervening matter, Crampton, Georgelin, and Georgelin (1978) have recently detected lines of Hα.

In this investigation we present new observations of W51 in the spectral lines of $\lambda = 2.6$ mm CO, $\lambda = 3.1$ mm CS, $\lambda = 2$ cm H_2CO, and the 2 cm recombination line H76α. The present study does not discuss the observations of the OH and H_2O masers (Morris 1976), the high-resolution interferometer results (Martin 1972; Scott 1978), or the near-infrared studies (Wynn-Williams, Becklin, and Neugebauer 1974). Those investigations concern the small-scale structure in W51; we, however, are primarily interested in the large-scale morphology and kinematics which reflect activity along the Sagittarius spiral arm.

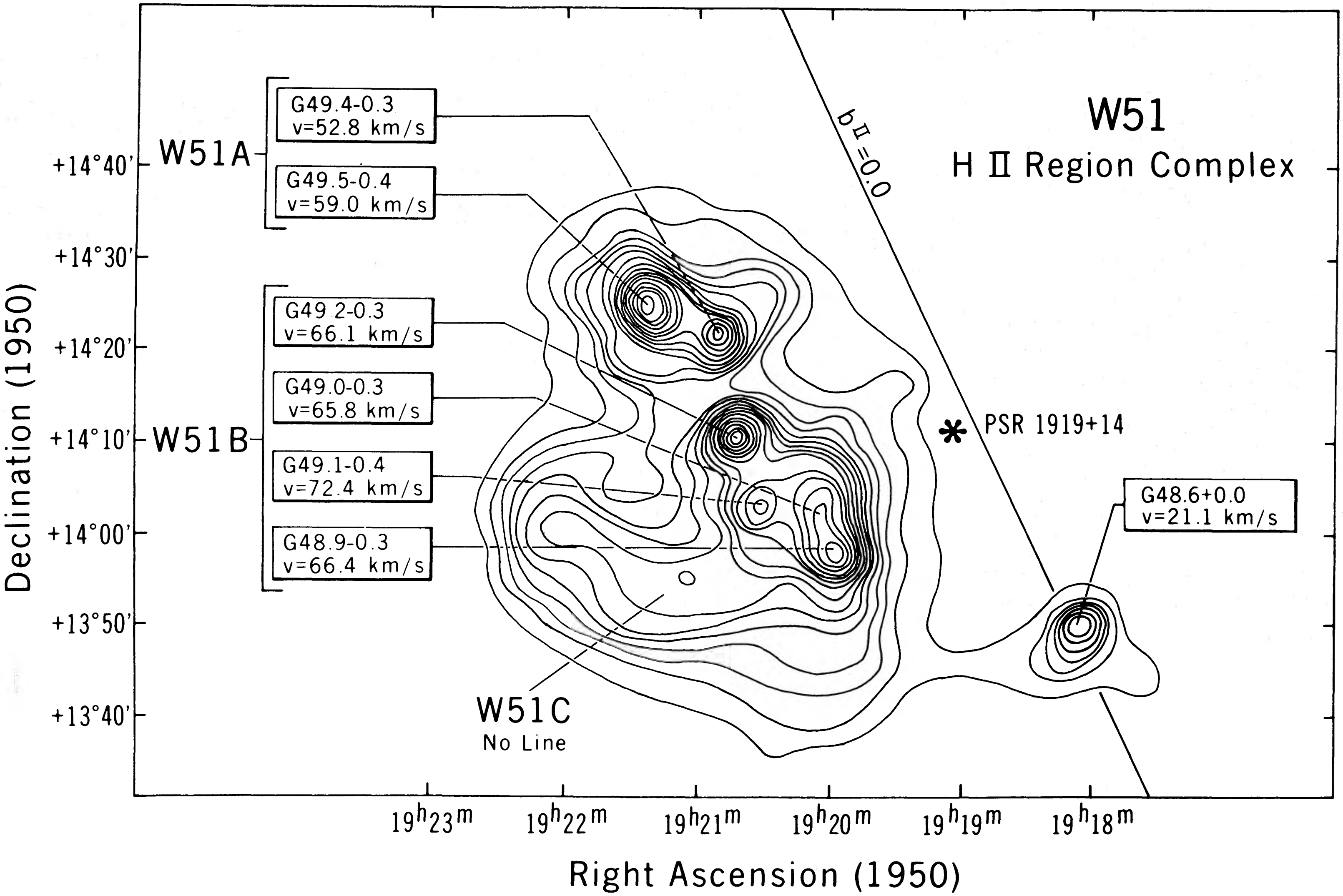

FIG. 1.—The W51 H II region complex. The 6 cm continuum contours are from Goss and Shaver (1970). The H109α recombination line velocity seen at each continuum peak has been taken from Wilson *et al.* (1970). The position of PSR 1919+14 is from Hulse and Taylor (1974).

II. OBSERVATIONS

Our carbon monoxide observations were obtained during 1974 April with the 11 m antenna on Kitt Peak, and the carbon monosulfide data were taken during 1976 October with this same instrument. The half-power beamwidth (HPBW) of this instrument is ~66″–77″ at the transition frequencies discussed here, 115.2712 GHz (^{12}CO), 110.2014 GHz (^{13}CO), and 97.9810 GHz (CS). During the CO observations, the noise temperature of the receiver was 1700 K (single sideband [SSB]), but the CS work was done with the newer cooled receiver which had a system temperature 900 K (SSB). Assuming that the individual source components of W51 have Gaussian brightness distributions of half-width between 3′ and 10′, we estimate the main beam efficiency to be approximately the value $\eta = 0.65$ (Ulich and Haas 1976). The uncertainty in the value of η introduced by the change from a prime-focus (CO) receiver to a Cassegrain (CS) receiver is small compared with the uncertainty introduced by variations in the size of the components.

All the carbon monoxide observations were made in a frequency-switching mode with an integration time of 5 minutes. The carbon monosulfide work was done by integrating on the source for 5 minutes and then switching the telescope to an OFF position 30′ east. For both sets of observations, filters of width 250 kHz were employed, giving velocity resolution 0.65 km s^{-1} (CO) or 0.76 km s^{-1} (CS). The spectra reported here are discussed in terms of the corrected antenna temperature $T_A{}^*$ defined by Ulich and Haas (1976), and so are corrected for atmospheric attenuation, blockage, and losses but not for geometric effects which describe the coupling of the detailed antenna beam response pattern to the source brightness distribution. At the G49.5−0.4 continuum peak, the value $T_A{}^* =$ 28.4 K for CO corresponds to an excitation temperature of the $J = 1$–0 transition of $T_E = 47$ K for an optically thick line (Ulich and Haas, eq. [13]). The rms fluctuation in $T_A{}^*$ is approximately 0.5 K for a single CO measurement and 0.2 K for CS.

The new recombination line and formaldehyde data reported here were taken with the 140 foot (43 m) telescope in Green Bank during 1975 July. At the transition frequencies of H76α (14.6900 GHz) and the 2_{11}–2_{12} transition of H_2CO (14.4885 GHz), the HPBW of this telescope is 2′ (cf. Paper I). The $\lambda = 2$ cm parametric amplifier we used gave a system temperature 100 K during our experiment, and all observations were taken in a total-power mode with, typically, 20 minute on-source integration times. The 384-channel autocorrelator was used in a parallel mode with a velocity resolution 0.65 km s^{-1} and total passband 250 km s^{-1}. As in Paper I, we corrected the data for the effects of gravitational distortion of the 140 foot telescope on its gain. The antenna temperatures given here for the $\lambda = 2$ cm observations should be correct to about 25%.

III. RESULTS

a) *Cold Gas*

The ^{12}CO spectra were taken at 1′ intervals on a square grid (in α, δ) of dimensions 12′ × 12′ about the peak of the 6 cm continuum flux in W51 A, G49.5−0.4; $\alpha(1950) = 19^h21^m25^s$, $\delta(1950) = 14°25'05''$ (Goss and Shaver 1970). We then mapped westward to include the second continuum source in W51 A, G49.4−0.3, at $\alpha(1950) = 19^h20^m54^s$, $\delta(1950) = 14°21'42''$ (Goss and Shaver). As time permitted, we mapped southward and westward toward W51 B. In Figure 2 we show most of the ^{12}CO spectra we obtained, superposed on the 6 cm continuum map of W51 A (Goss and Shaver). In this figure the antenna temperatures have been normalized so that $T_A{}^* =$ 28.4 K at the center of G49.5−0.4, in accordance with the calibration of Ulich and Haas (1976). The ordinates and abcissae are given in terms of the offsets, in arcminutes, from G49.5−0.4; the radial velocity scale (with respect to the local standard of rest [LSR]) for each spectrum is shown at the bottom. Adopting a distance of 6.5 kpc to W51 (Reifenstein *et al.* 1970), the figure covers a physical grid of size ~34 pc × 34 pc.

The carbon monoxide spectra can generally be decomposed into individually traceable velocity components near 52, 58, and 65–70 km s^{-1}, each of which can be associated in position with one or more peaks in the thermal continuum emission. This is illustrated in Figure 3, a spatial-velocity diagram constructed along the northeast-southwest ($\Delta\alpha = \Delta\delta$) line through the center of G49.5−0.4. Positions of closest approach of this line to several G components in W51 A and B are also noted (cf. Fig. 1). The H109α recombination line velocity seen in each G component is given in parentheses. Figure 3 shows clearly an emission feature at 52 km s^{-1} that peaks near G49.4−0.3 and G49.5−0.4 and an emission feature at 58 km s^{-1} that peaks near G49.5−0.4. In addition, there is a spectral feature near 66 km s^{-1} that appears in emission in W51 B (G49.2−0.3, G49.1−0.4) but shows itself as a dip in the emission at G49.5−0.4 in W51 A.

The suppression of ^{12}CO emission in the neighborhood of G49.5−0.4 is shown more clearly in Figure 4; here we give the ^{12}CO and ^{13}CO spectra, as well as their ratio, at the G49.5−0.4 continuum peak and at two other representative points within the nebula. The ratio ^{12}CO/^{13}CO at the 52 and 58 km s^{-1} peaks suggests that $\tau(^{13}\mathrm{CO}) < 1$. The high-velocity shoulder seen in these optically thin ^{13}CO spectra (Figs. 4*a* and 4*b*) suggests the occurrence of an emission feature at 66 km s^{-1}. The ^{12}CO spectra, however, show that the emission from gas at this velocity has been suppressed. Away from G49.5−0.4, the optically thin ^{13}CO still shows a high-velocity feature (Fig. 4*c*). Here, though, the ^{12}CO spectrum also has emission at the same velocity.

The velocity of the three molecular emission features in the W51 complex can be understood within the context of the morphology of galactic H I and ^{12}CO emission in the range $l^{\mathrm{II}} = 49°$–50°. The galactic ^{12}CO emission in this longitude range at $b^{\mathrm{II}} = 0°$ is given in Figure 5 (Burton and Liszt 1979) for comparison with the distribution of

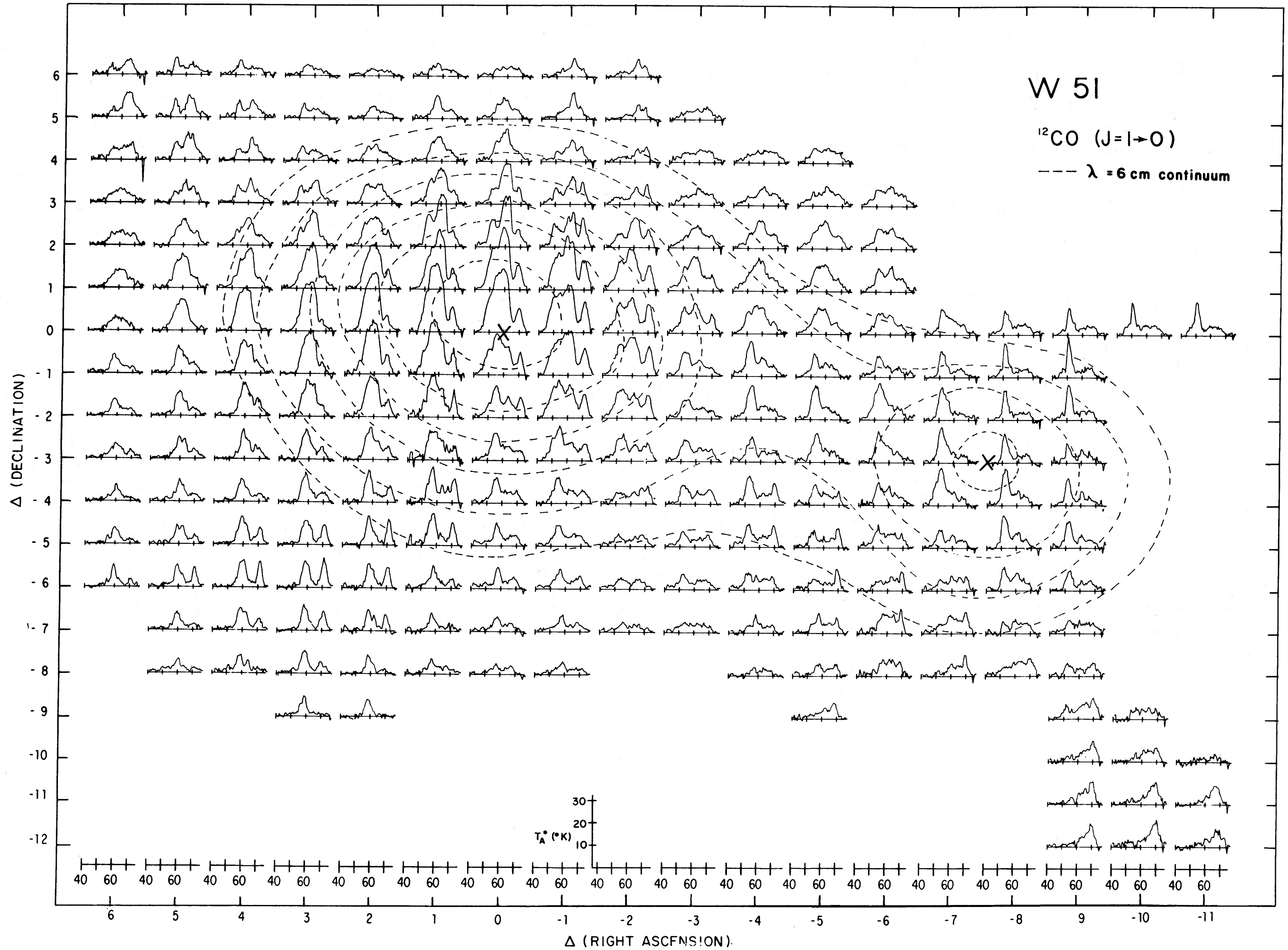

FIG. 2.—The ^{12}CO spectra of the W51 A complex superposed on the 6 cm continuum map of Goss and Shaver (1970). All antenna temperatures have been normalized to $T_A^* = 28.4$ K at the 6 cm continuum peak. The ordinates and abscissae are given in terms of the offsets from the G49.5−0.4 peak. The radial velocity scale for each spectrum is shown at the bottom.

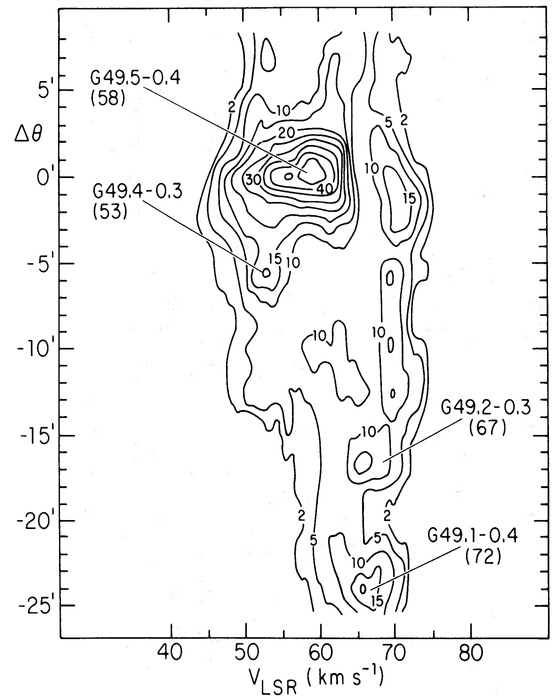

FIG. 3.—Spatial-velocity map of the ^{12}CO intensity constructed along the northeast-southwest ($\Delta\alpha = \Delta\delta$) line through the 6 cm continuum peak of G49.5−0.4. Contours are labeled by values of $T_A^*/\eta = T_B$. Positions of closest approach of this line to several G components in W51 A and B are noted (Wilson *et al.* 1970). The H109α recombination line velocity for each G component is also given.

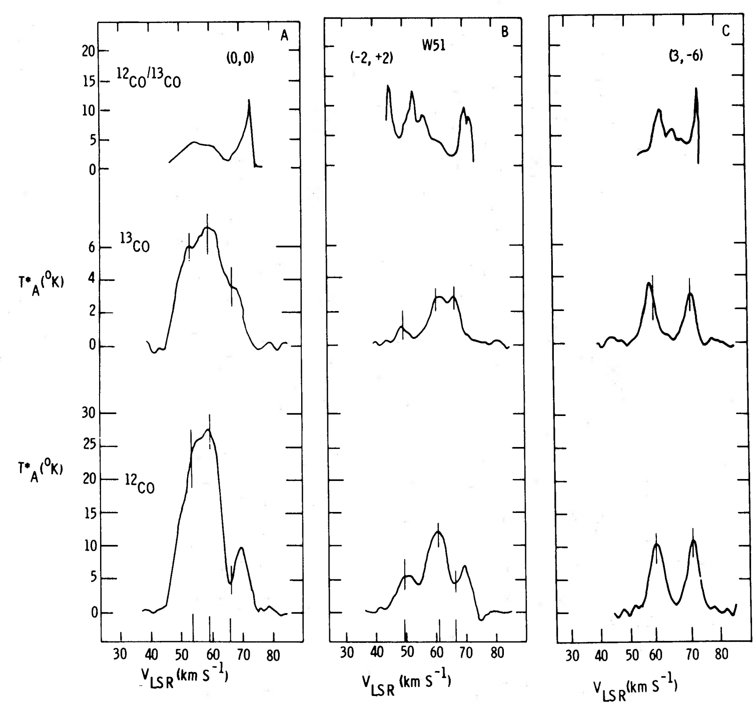

FIG. 4.—The observed ^{12}CO and ^{13}CO spectra of W51 and the ratio of the intensities of these lines at three positions within the nebula: (*a*) the 6 cm continuum peak of G49.5−0.4; (*b*) 2′ west and 2′ north; and (*c*) 3′ east and 6′ south of this peak.

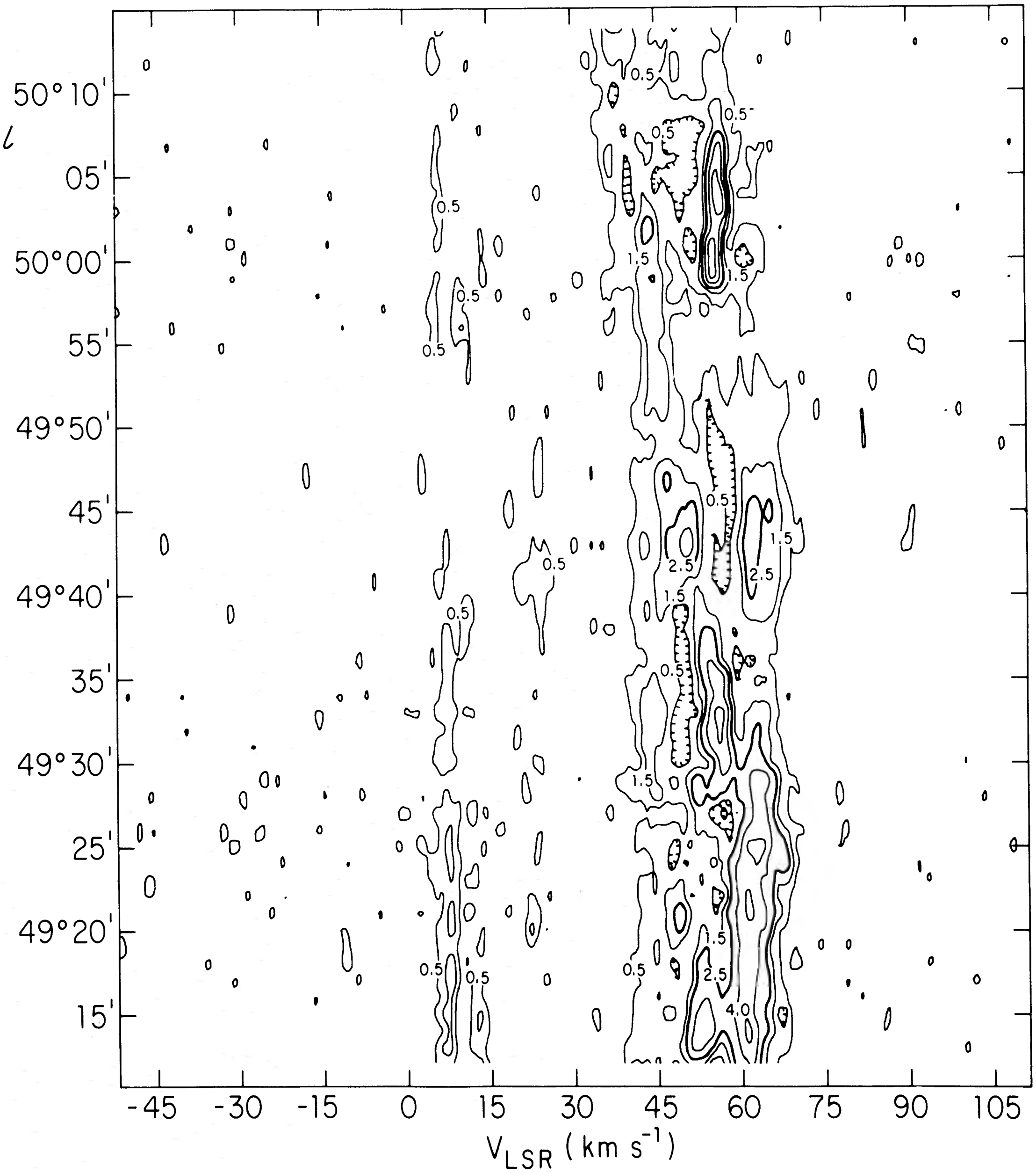

FIG. 5.—Galactic longitude–velocity map ($b^{II} = 0$) of the ^{12}CO emission in the neighborhood of W51 from Burton and Liszt (1979). The intensity contours are labeled by $T_A^*/\eta = T_B$. The contour levels are 0.5, 1.5, 2.5, 4 K, and are then incremented by 1.5 K thereafter.

H I shown by Burton (1970*b*). In the neighborhood of the W51 complex, the 21 cm emission profiles show three streams of cold gas. The high-velocity stream at 66 km s^{-1} appears as a rather localized feature, which is strong only near the W51 complex. The two other H I streams, those with velocities of 52 and 58 km s^{-1} at W51, are features widely distributed in the Sagittarius spiral arm. In Figure 5 the localized high-velocity stream, as well as the two widely distributed lower-velocity streams, can be seen near the longitude of the W51 complex. Studies of the distribution of ^{12}CO in the galactic plane (Burton *et al.* 1975) also show that the high-velocity stream is local to the W51 complex. In addition, Figure 5 shows the patchy nature of the two lower-velocity streams. The typical diameter of one of these cold clumps of ^{12}CO is 10′ (20 pc), and that is the approximate size of the core of the dense cloud near G49.5−0.4.

Burton and Shane (1970) have suggested that the kinematics of the high-velocity gas in this region can be understood in terms of streaming motions of order 7–10 km s^{-1} superposed on the basic circular galactic rotation speed of 55 km s^{-1}. These streaming motions might be the result of the passage of a density-wave shock through the region (Roberts 1969; Woodward 1975). The high-velocity stream (Fig. 5) then arises behind an arclike material condensation, i.e., the Sagittarius spiral arm, at distances 6–8 kpc from the Sun. The presence of H I (Burton 1970*b*; Radhakrishnan *et al.* 1972) and strong H_2CO (Bieging 1975) absorption against both W51 A and B at velocities greater than those permitted by galactic rotation suggests that both sources are beyond the subcentral point. Bieging has argued that the weakness of H_2CO absorption at 67 km s^{-1} absorption places G49.4−0.3 closer to the Sun than to the subcentral point. However, we believe this to be improbable; more likely, the weak absorption is an artifact of the patchy distribution of the molecular gas.

i) *Cold Gas within W51 A*

In Figure 6 we show a radial velocity–right ascension map of the ^{12}CO emission spectra superposed on a similar map of the 6 cm (1_{10}–1_{11}) H_2CO absorption spectra of Scoville and Solomon (1973). The right ascension cut is through the center of the continuum source G49.5−0.4. Figure 6 shows that there are three peaks in the ^{12}CO emission: at 52 km s^{-1} (to the west), 58 km s^{-1}, and 70 km s^{-1}. The absence of emission at 66 km s^{-1} is apparent

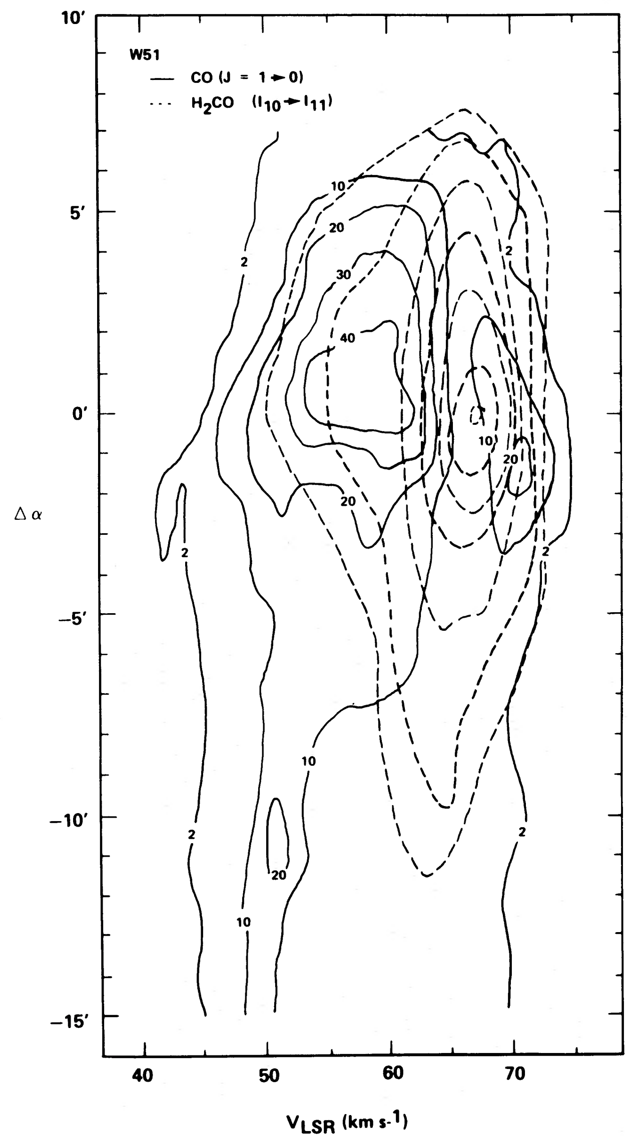

FIG. 6.—*Solid contours*, velocity position map of the intensity of the ^{12}CO line in a right ascension cut through the 6 cm continuum peak of G49.5−0.4. The contours are labeled by values of $T_A{}^*/\eta = T_B$. *Dashed contours*, velocity position map of the 6 cm (1_{10}–1_{11}) H_2CO absorption spectra of Scoville and Solomon (1973). The central contour is −30 K. The contours are shown every −5 K.

here. However, the 6 cm H_2CO contours show a deep absorption feature at 66 km s^{-1}, the velocity at which the ^{12}CO line flux exhibits a local minimum. In addition, the H_2CO spectra have broad wings on their low-velocity side, suggesting a weaker spectral feature near 58 km s^{-1}. Any absorption near 52 km s^{-1} is very weak. Figure 6 is consistent with the occurrence of three kinematic components of cold gas near G49.5−0.4: at 52 km s^{-1}, 58 km s^{-1}, and 66 km s^{-1}. Emission at 66 km s^{-1} from the ^{12}CO is suppressed by cold gas in the high-velocity stream lying in front of G49.5−0.4.

What is the nature then of the ^{12}CO emission at 70 km s^{-1} seen in Figure 6? Scoville and Solomon (1973) argued that the 70 km s^{-1} emission is the line wing of the broad feature at 58 km s^{-1}. However, we feel this explanation to be unlikely. Were the 70 km s^{-1} emission always to be regarded as an artifact of absorption, then this high-velocity line wing would be correlated at all positions with emission at 58 km s^{-1}. Figure 2 shows this not to be the case. Further, there appears to be little evidence in observations of any molecular species for the presence of a component which is so broad in velocity that it could be centered much below 66 km s^{-1} and still emit strongly enough in the far line wings that foreground absorption could create the 70 km s^{-1} feature. More likely, the site of the gas emitting at 70 km s^{-1} is the high-velocity stream itself. The ^{12}CO spectra (Figs. 2 and 4), the H_2CO spectra (Scoville and Solomon; Bieging 1975), and the OH spectra (Slysh 1974) all show evidence for patchiness in the high-velocity stream. In particular, there is an absorption feature at 63 km s^{-1} near G49.4−0.3 observed in both H_2CO and OH. The 70 km s^{-1} gas might also be a small clump in the high-velocity stream. The presence of the strong continuum source G49.5−0.4 near the high-velocity stream could increase the temperature of the foreground gas at 70 km s^{-1}, thus exciting both ^{12}CO and ^{13}CO emission. In this case the geometry of W51 A would be similar to that of W49 A (Paper I), where an H II region is found between two molecular clouds.

To assess the degree to which foreground absorption modifies the appearance of molecular emission profiles taken toward G49.5−0.4, we mapped the 2_{11}–2_{12} line of H_2CO and the J = 2–1 line of CS around this source. The first of these transitions affords a means of studying the foreground material at relatively high spatial resolution (2′), while the other preferentially samples regions of higher density. Maps of these species, again superposed on the east-west ^{12}CO distribution, are given in Figures 7 and 8.

The H_2CO absorption was mapped at positions 1′ and 2′ to the north, south, east, and west of G49.5−0.4. Figure 7 again shows the presence of the deep absorption feature in H_2CO at 66 km s^{-1} where the ^{12}CO emission has a minimum. A weaker feature at 58 km s^{-1} is now apparent, as well as some absorption at 52 km s^{-1}. We have decomposed our 2 cm H_2CO into two components at 58 and 66 km s^{-1}, and compared the ratio of their strengths. This ratio, which shows a minimum near the G49.5−0.4 continuum peak, suggests that the high-velocity stream (cloud I, Fig. 10) is in front of the G49.5−0.4 continuum sources and the molecular cloud at 58 km s^{-1} (cloud II, Fig. 10) is behind G49.5−0.4. In this picture the 58 km s^{-1} cloud is seen in anomalous absorption. But the 6 cm absorption at 58 km s^{-1} observed by Wilson *et al.* (1976) seems too strong to be attributable to anomalous absorption alone. More likely, some of the small dense knots of ionized gas observed in G49.5−0.4 (Martin 1972; Scott 1978) are embedded within a patchy 58 km s^{-1} molecular cloud while the bulk of the ionized gas is located at the front surface of the neutral material. Kinematically, the third cold cloud at 52 km s^{-1} (cloud III, Fig. 10) is located behind the W51 continuum sources. Fomalont and Weliachew (1973) have synthesized the 6 cm H_2CO distribution about G49.5−04, and find a deep absorption feature in the velocity interval 60.7–70.0 km s^{-1}

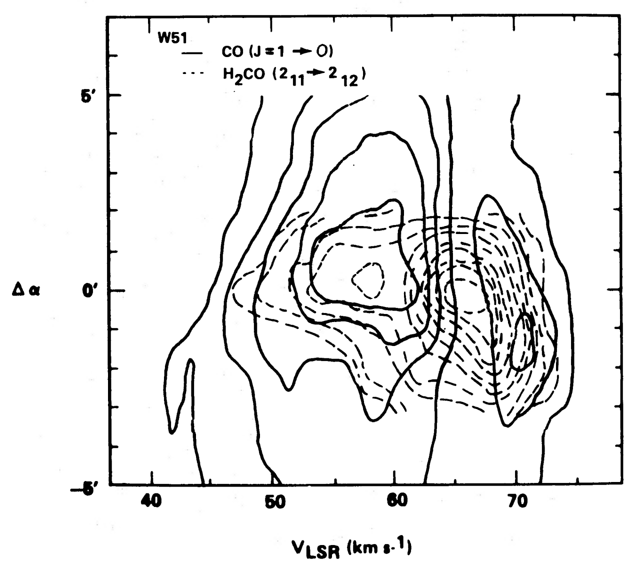

FIG. 7.—*Solid contours*, as in Fig. 5. *Dashed contours*, velocity position map of the 2 cm (2_{11}–2_{12}) H_2CO absorption spectra. The central contour is −9.6 K. The contours are shown every −2 K.

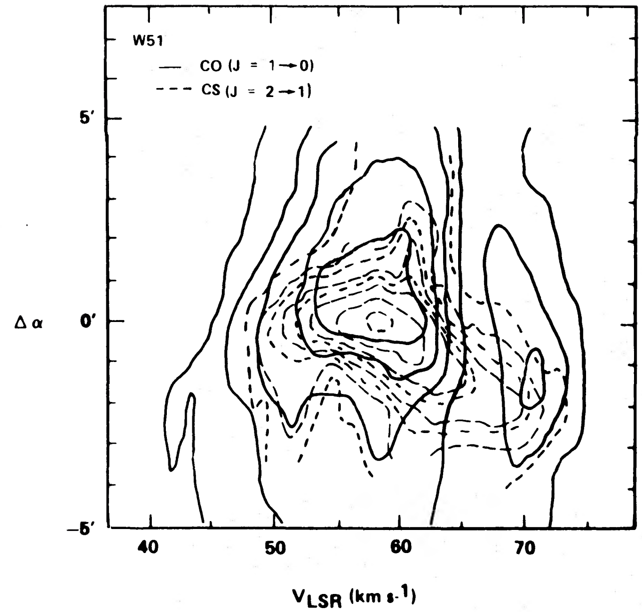

FIG. 8.—*Solid contours*, as in Fig. 5. *Dashed contours*, velocity position map of the ^{12}CS (J = 2–1) emission spectra. The central contour is 18 K. The contours are shown every 2 K.

and a weaker absorption feature in the interval 54.6–60.7 km s^{-1}. The intensity distribution they found in the two velocity intervals is consistent with our discussion of the 2 cm H_2CO spectra. Our placement of the three molecular streams in W51 also agrees well with the conclusions drawn by Scoville and Solomon (1973).

In Figure 8, where the ^{12}CS (J = 2–1) spectra are shown, we again find emission components at 52 and 58 km s^{-1} near G49.5−0.4. However, unlike the comparison ^{12}CO spectra, the ^{12}CS spectra have emission at 66 km s^{-1} to the west of G49.5−0.4. In contrast, the ^{12}CS (J = 1–0) spectra of Turner *et al.* (1973) and the ^{12}CO (J = 2–1) spectra of Goldsmith, Plambeck, and Chiao (1975) do have suppressed emission at 66 km s^{-1}. These data imply that suppressed emission is the result of differences in molecular line opacity and can be used as a probe into the physical conditions of the high-velocity stream. This conclusion is reinforced by the 66 km s^{-1} emission observed in the molecular species with still lower opacity: ^{12}CS (J = 3–2) (Penzias *et al.* 1971) and HCN (Snyder and Buhl 1971).

b) *Ionized Gas*

Implicit in our study of W51 is the assumption that the molecular gas clouds are only part of a complex that also includes large H II regions and newly formed stars. To probe the continuum sources of the W51 complex, we mapped the H76α recombination line at positions 1′ and 2′ to the north, south, east, and west of the G49.5−0.4 continuum peak. In Table 1 we give the result of our observations of the H76α recombination line at G49.5−0.4. In addition, we give the other α recombination line data we have for the W51 complex. The data have been specified for both continuum sources in W51 A and two of the continuum sources in W51 B. This table lists N, the principal quantum number of the transition; its LSR velocity; the line-to-continuum ratio; the full width at half-maximum (FWHM) of a Gaussian fit to the line ($\Delta\nu$); and the source of the observations. From the LSR velocities listed in Table 1, the continuum sources labeled W51 B can most likely be associated with the high-velocity stream; G49.5−0.4 with the 58 km s^{-1} cloud; and G49.4−0.3 with the 52 km s^{-1} cloud. The line widths of all the α recombination lines in the continuum sources observed are consistent with a thermal gas with a kinetic temperature $T \approx$ 1.0–1.3 × 10^4 K. For $N < 166$, the recombination lines appear to form in ionized gas with a density $n \approx 10^3$–10^4 cm^{-3}. The H221α and H247α recombination lines seen in G49.5−0.4 and W51 B, however, imply the existence of low-density ionized gas, $n \approx 50$ cm^{-3} (Paper I). If G49.5−0.4 and W51 B are near the outside of a cold cloud, then the gas ionized by young stars will be found somewhere in the low-density regions between the clouds. The low-frequency continuum emission in W51 (Parrish 1972) is additional evidence that low-density ionized gas is associated with the molecular gas, most probably in the large volume between the cold clouds. Models of the ionized gas distribution (§ IV and Table 3) confirm the existence of this extended region of low-density ionized gas.

Since the depth of absorption in H_2CO shows a minimum at 66 km s^{-1} at the position of G49.2−0.3 in W51 B (Scoville and Solomon 1973), W51 B can be placed behind the high-velocity stream. Kinematically, then, the entire W51 H II region complex lies behind the high-velocity stream. The H_2CO profiles at G49.5−0.4 suggested that the 58 km s^{-1} cloud was seen in anomalous absorption, requiring most of the G49.5−0.4 continuum sources to be

TABLE 1

PARAMETERS OBSERVED IN THE HYDROGEN RECOMBINATION LINES OF W51

Transition	V_{LSR} (km s^{-1})	T_L/T_c	$\Delta\nu$ (km s^{-1})	Reference
		W51 A: G49.5−04		
H66α	56.8 ± 1.5	0.27 ± 0.06	26.8 ± 3.6	Waltman and Johnston 1973
H73α	57.0 ± 2.0	0.11 ± 0.04	26.8 ± 4.0	Papadopoulos *et al.* 1972
H76α	58.0 ± 2.0	...	29.8 ± 4.0	This paper
H76α	57.5 ± 3.5	...	29.9 ± 2.0	Gull and Balick 1974
H92α	59.7 ± 1.5	...	...	Chaisson 1974
H109α	58.2 ± 0.6	(4.1 ± 0.9) × 10^{-2}	31.7 ± 6.0	Reifenstein *et al.* 1970
H109α	59.0 ± 3.0	(4.9 ± 0.1) × 10^{-2}	36.7 ± 5.3	Wilson *et al.* 1970
H109α	58.4 ± 0.9	...	31.0 ± 6.0	Palmer *et al.* 1969
H126α	55.0 ± 3.0	(4.2 ± 1.8) × 10^{-2}	37.0 ± 8.3	McGee and Gardner 1968
H134α	58.6 ± 0.9	(1.9 ± 0.3) × 10^{-2}	33.1 ± 1.5	Zuckerman and Palmer 1970
H157α	59.0 ± 2.0	(1.5 ± 0.04) × 10^{-2}	35.3 ± 3.5	Churchwell and Edrich 1970
H158α	57.6 ± 3.6	...	25.0 ± 6.0	Dieter 1967
H159α	56.0 ± 1.0	(1.2 ± 0.06) × 10^{-2}	36.5 ± 3.7	Churchwell and Edrich 1970
H221α	58.9 ± 4.2	(1.9 ± 0.6) × 10^{-3}	31.6 ± 9.6	Pankonin *et al.* 1974
H247α/H248α	54.6 ± 2.7	(1.8 ± 0.3) × 10^{-3}	31.3 ± 6.9	Pankonin *et al.* 1974
		W51 A: G49.4−0.3		
H76α	54.6 ± 3.3	...	30.4 ± 2.0	Gull and Balick 1974
H109α	52.8 ± 3.3	(4.8 ± 0.6) × 10^{-2}	30.0 ± 5.4	Wilson *et al.* 1970
		W51 B: G49.0−0.3		
H109α	63.2 ± 3.6	(5.3 ± 2.2) × 10^{-2}	25.3 ± 3.6	Reifenstein *et al.* 1970
H109α	65.8 ± 4.2	(5.5 ± 2.4) × 10^{-2}	28.9 ± 7.2	Wilson *et al.* 1970
H158α	62.0 ± 1.2	(9.7 ± 1.2) × 10^{-3}	26.2 ± 2.6	Dieter 1967
H166α	...	(1.1 ± 0.44) × 10^{-2}	28.3 ± 5.6	Pedlar and Davies 1972
H192α	56.6 ± 1.0	(4.6 ± 0.52) × 10^{-3}	21.3 ± 2.0	Pedlar and Davies 1972
H220α	58.3 ± 2.3	(2.9 ± 0.3) × 10^{-3}	35.4 ± 2.9	Pedlar and Davies 1972
H257α	58.0 ± 4.0	(1.7 ± 0.5) × 10^{-3}	32.5 ± 8.5	Gordon *et al.* 1974
		W51 B: G49.2−0.3		
H109α	67.2 ± 4.2	(7.7 ± 4.2) × 10^{-2}	30.3 ± 8.7	Reifenstein *et al.* 1970
H109α	66.1 ± 5.4	(5.2 ± 2.4) × 10^{-2}	46.3 ± 16	Wilson *et al.* 1970

NOTE.—All errors are 3 σ.

located in front of the 58 km s^{-1} cold gas. On the basis of their analysis of the H_2CO profiles, Scoville and Solomon also argued that G49.5−0.4 is on the cloud side nearest to W51 B. This result also follows from our observations of the H76α recombination line. In Figure 9, where we show the mean velocity of the ionized gas near G49.5−0.4, we find that the center velocity of the H76α line increases quite rapidly to the south and west of the continuum peak, reaching 64 km s^{-1} only 2′ away. Such behavior is also observed in CS (Fig. 8). Apparently, ionized gas from G49.5−0.4 is exciting the CS in the cold gas of the high-velocity stream, placing W51 A between the 58 km s^{-1} cloud and the high-velocity stream.

c) W51 C

The location of W51 C, or the eastern arm, has not yet been specified. Since no recombination lines have been observed in W51 C, Wilson *et al.* (1970) conclude that this source, like W49 B (Mezger, Schraml, and Terzian 1967), is nonthermal. Hulse and Taylor (1974) suggested that the newly discovered pulsar PSR 1919+14 was associated with the nonthermal W51 C 5 GHz radio contours. But PSR 1919+14 is considerably displaced from the eastern arm as can be seen in Figure 1. Its distance of 2.5 kpc (Hulse and Taylor) also places it far from the W51 complex. If the W51 B continuum region is a group of stars near the back of the high-velocity stream, then W51 C may be ionized (that is, thermal) gas streaming into the regions between neutral clouds I and II. The absence of recombination line emission would then be the result of two effects. The density of material falls, and thus the intensity of line emission relative to continuum emission falls as the ionized gas streams outward. In addition, the velocity of the gas increases as it moves into regions of lower density (Paper I). This tends to broaden the profile and further decrease the intensity of line emission. The observation that the ionized gas nearest W51 C has an H109α recombination line velocity of 72.4 km s^{-1} (Wilson *et al.* 1970) can then be explained.

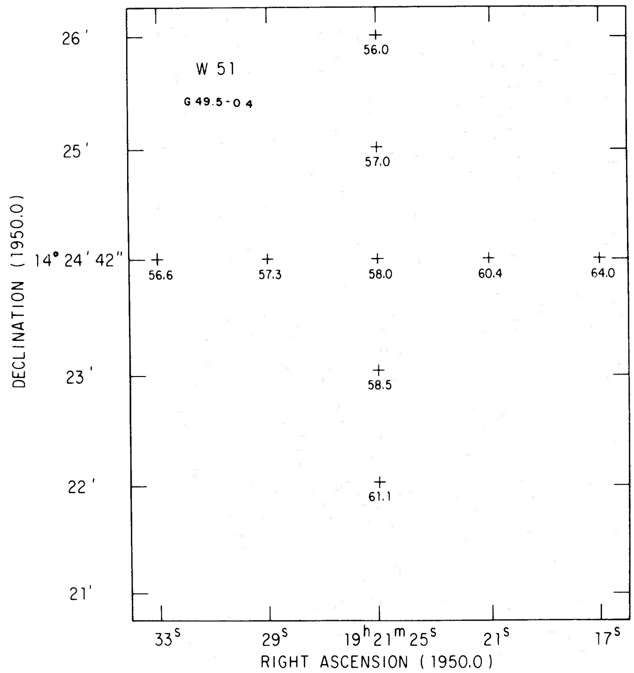

FIG. 9.—Position map of the velocity of the ionized gas in the neighborhood of G49.5−0.4

d) *The W51 Complex*

We believe that the observational data we have presented are consistent with the picture of the W51 H II region–molecular cloud complex given in Figure 10. In this figure the three molecular clouds, as viewed from the Earth, have been represented schematically by three slabs of cold gas. The W51 B and G49.5−0.4 continuum complexes have been placed between clouds I and II, and G49.5−0.3 lies nearest cloud III. Ionized gas from G49.5−0.4 and W51 B streaming into the low-pressure regions between clouds I and II is responsible for the low-frequency radio emission and high-N recombination lines.

In Figure 10 we have also tried to place the W51 complex within the galactic spiral structure. The schematic representation of the spiral structure is after Lin (1971). The location of the W51 complex within the Sagittarius spiral arm is after Burton and Shane (1970).

IV. H II REGIONS IN W51

Our present discussion of the structure of the W51 complex and our previous results concerning W49 A (Paper I) have suggested that large H II regions are feeding ionized gas into the large volume between gas clouds. In particular, the low-frequency line and continuum observations of the H II regions associated with these complexes require low-density ionized gas. If H II regions should form near the outside of clouds, then this low-density ionized gas would be a consequence of ionized gas streaming into the regions between the clouds.

One requirement of our picture, then, is the presence of low-density ($n \approx 50\ \mathrm{cm}^{-3}$) ionized gas within the W51 complex. To test this hypothesis, we have constructed simple models that reproduce the observations of the H II regions in W51. The data used in the models are given in Tables 1 and 2. For the present computations we have described H II regions by 10 concentric shells of ionized gas. In addition to hydrogen, the nebular gas consisted of 10% singly ionized He by number. Within each shell the conditions of density and temperature were homogeneous. The procedure used in these computations closely follows the methods outlined in Paper I. The total continuum flux density is given by

$$S_\nu^c = \frac{1}{d^2}\int_{\mathrm{HPBW}} I_\nu^c \quad (\phi) P_n(\phi) 2\pi\phi d\phi\,, \tag{1}$$

where d is the distance to the nebula, $I_\nu^c(\phi)$ is the intensity in the continuum, $P_n(\phi)$ is the normalized antenna response pattern, $\phi = r/d$ is the angular extent of radius r measured at the Earth, and the integration is over the HPBW of the telescope. In this relation the antenna response pattern is normalized so that $P_n(0) = 1$ (Kraus 1966). In the calculations the HPBW of the 140 foot Green Bank telescope was used for $\nu > 1.4$ GHz (Lockman and Brown 1976), with the addition that HPBW $= 10'$ at $\nu = 1.4$ GHz (Pauliny-Toth, Wade and Heeschen 1966).

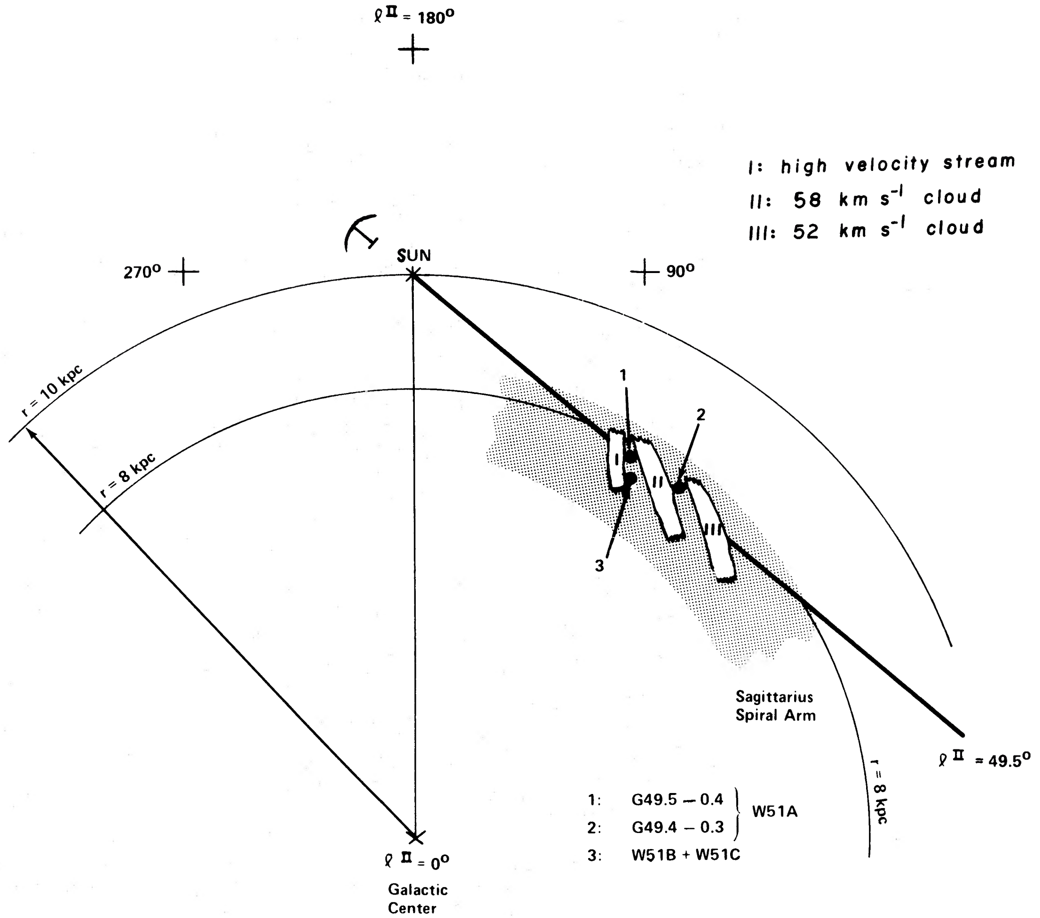

FIG. 10.—Schematic representation of the W51 H II region–molecular cloud complex. The representation of the spiral structure is after Lin (1971), and the location of the W51 complex within the Sagittarius spiral arm is after Burton and Shane (1970).

For $\nu < 1.4$ GHz, the HPBW of the Arecibo 1000 foot (305 m) telescope was used (Terzian and Balick 1969; Parrish 1972). The continuum intensity is given by

$$I_\nu{}^c(\phi) = \sum_{i=m}^{10} \left\{ \frac{2kT_i}{c^2} \nu^2 [1 - \exp(-\kappa_i{}^c r_i)] \left[\prod_{j=i+1}^{10} \exp(-\kappa_j{}^c r_j) + \prod_{j=m}^{i-1} \exp(-\kappa_j{}^c r_j) \prod_{j=m}^{10} \exp(-\kappa_j{}^c r_j) \right] \right\}, \quad (2)$$

where T_i and r_i are the temperature and radius of the ith shell, and $\kappa_i{}^c$ is the continuum absorption coefficient in this shell (Brocklehurst and Seaton 1972). If ϕ_i is the angular radius of the ith shell, then m designates the first shell for which

$$\phi_m - \phi > 0 . \quad (3)$$

For $i + 1 > 10$, the first product in equation (2) was set to 1. For $i - 1 < m$, the second product in equation (2) was set to 1.

The results of the computations of the continuum flux density are shown in Figure 11. In this figure, models of four continuum sources are shown with the observed continuum flux densities superposed. The data for the four sources are given in Table 2. In this table the W51 complex has been separated into the components W51 A, W51 B, and the envelope source; W51 A has been further separated into G49.5−0.4 and G49.4−0.3. The envelope source is the continuum emission seen from the entire complex at low frequencies. Table 2 lists for each component the frequency of the observation, the corrected central flux density in janskys, and the reference for the observations. The corrected central flux density is given by $S = 2k\nu^2 T_B / c^2 \Omega_S \eta$, where T_B is the brightness temperature of the source, Ω_S is the source solid angle, and the telescope efficiency $\eta = 1/(1 + \Omega_A/\Omega_S)$ (Ω_A is the beam solid angle).

The parameters used in the construction of the models are given in Table 3. For the four continuum sources, this table lists the radius and density of the 10 concentric shells; the isothermal kinetic temperature T and distance d chosen for the H II region; and the number of ionizing photons per second, S_0, required to keep the gas ionized.

TABLE 2

Parameters of the Observed Continuum Emission in W51

Frequency (GHz)	Corrected Central Flux (Jy)	Reference
W51 A: G49.5−0.4		
15.4	96 ± 6	Schraml and Mezger 1969
10.7	93 ± 9	MacLeod and Doherty 1968
5.0	115 ± 17	Goss and Shaver 1970
5.0	117 ± 18	Wilson *et al.* 1970
5.0	109 ± 16	Altenhoff *et al.* 1970
5.0	109 ± 20	Gardner and Morimoto 1968
2.7	119 ± 18	Altenhoff *et al.* 1970
1.414	100 ± 15	Altenhoff *et al.* 1970
0.408	53.2 ± 7.8	Goss and Shaver 1970
0.408	43 ± 6.4	Shaver 1969
W51 A: G49.4−0.3		
15.4	20 ± 1.2	Schraml and Mezger 1969
10.7	22 ± 2	MacLeod and Doherty 1968
5.0	27.8 ± 5	Gardner and Morimoto 1968
5.0	33.4 ± 5	Wilson *et al.* 1970
5.0	37.2 ± 6	Goss and Shaver 1970
0.408	18 ± 2.7	Shaver 1969
0.408	22.7 ± 3.4	Goss and Shaver 1970
W51 B		
15.4	82.5 ± 5	Schraml and Mezger 1969
10.7	129.5 ± 13	MacLeod and Doherty 1968
5.0	137 ± 21	Wilson *et al.* 1970
2.315	230 ± 50	Kundu and Velusamy 1967
1.430	190 ± 60	Kundu and Velusamy 1967
1.400	366 ± 50	Pauliny-Toth *et al.* 1966
0.611	397 ± 60	Terzian and Balick 1969
0.6105	415 ± 83	Wendker and Yang 1968
0.430	185 ± 30	Kundu and Velusamy 1967
0.430	243 ± 50	Terzian and Balick 1969
0.408	310 ± 31	Shaver 1969
Envelope Source = W51 A + B + C		
1.400	576 ± 86	Pauliny-Toth *et al.* 1966
0.750	493 ± 74	Pauliny-Toth *et al.* 1966
0.611	509 ± 78	Terzian and Balick 1969
0.430	322 ± 65	Terzian and Balick 1969
0.195	383 ± 76	Terzian and Balick 1969
0.195	220 ± 60	Kundu and Velusamy 1967
0.089	288 ± 30	Parrish 1972
0.074	170 ± 25	Parrish 1972
0.065	150 ± 20	Parrish 1972
0.053	72 ± 30	Parrish 1972

Note.—All errors are 3 σ.

The large volume of low-density gas required to reproduce the low-frequency continuum observations should be particularly noted. The continuum models were found not to be very sensitive to the choice of temperature within the range $T = 8$–15×10^3 K.

In Figure 12 we show computations of the integrated line-to-continuum ratio for the two H II regions where enough observational data exist to compare with the theory: G49.5−0.4 and G49.0−0.3. The model for G49.5−0.4 was taken from Table 3, and a separate model was constructed for G49.0−0.3. The observed values were taken from Table 1. The integrated line-to-continuum ratio was calculated from the relation

$$\frac{T_L \Delta\nu}{T_c \nu^2} = \frac{\int_{\text{FWHM}} d\nu \int_{\text{HPBW}} [I_\nu^{L+c}(\phi) - I_\nu^c] P_n(\phi) 2\pi\phi d\phi}{\nu^2 \int_{\text{HPBW}} I_\nu^c(\phi) P_n(\phi) 2\pi\phi d\phi}, \tag{4}$$

where $I_\nu^{L+c}(\phi)$ is the line-plus-continuum intensity and the frequency integral is taken over the FWHM of the

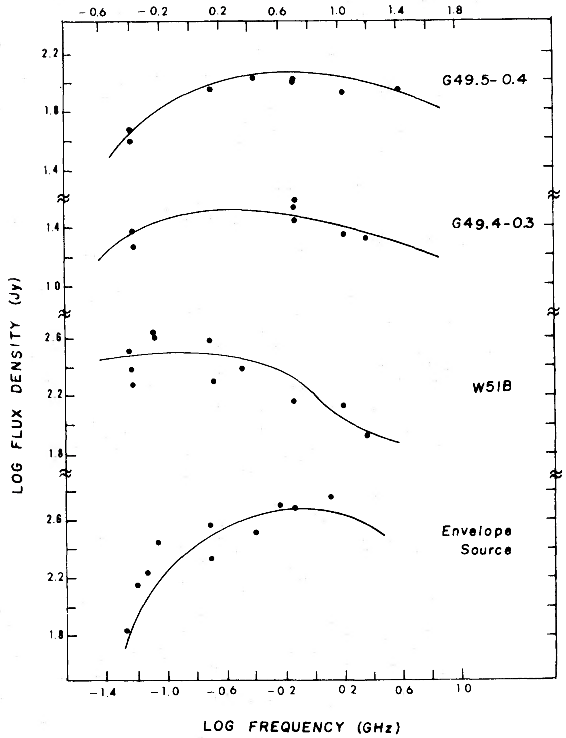

FIG. 11.—The continuum flux density predicted by models of the H II regions within the W51 complex (Table 3). The observations of the continuum flux density (Table 2) are superposed onto the calculated curves. The frequency scale at the top refers to the top three models. The frequency scale at the bottom refers to the envelope source.

Doppler-broadened line core at the isothermal H II region temperature $T_D = 2T_i$. The intensity in the line plus continuum is given by

$$I_\nu^{L+c}(\phi) = \sum_{i=m}^{10} \frac{2kT_i}{c^2} \nu^2 \left(\frac{\kappa_i^c + b_N\kappa_i^L}{\kappa_i^c + b_N\beta_N\kappa_i^L}\right)\{1 - \exp[-(\kappa_i^c + b_N\beta_N\kappa_i^L)r_i]\}$$
$$\times \left\{\prod_{j=i+1}^{10} \exp[-(\kappa_j^c + b_N\beta_N\kappa_j^L)r_j] + \prod_{j=m}^{i-1} \exp[-(\kappa_j^c + b_N\beta_N\kappa_j^L)r_j]\prod_{j=m}^{10} \exp[-(\kappa_j^c + b_N\beta_N\kappa_j^L)r_j]\right\} . \quad (5)$$

TABLE 3

MODEL PARAMETERS FOR THE H II REGIONS IN W51

	G49.5−0.4		G49.4−0.3		W51 B		ENVELOPE SOURCE		G49.0−0.2	
SHELL	r (pc)	n (cm^{-3})	r (pc)	n (cm^{-3})	r (pc)	n (cm^{-3})	r (pc)	n (cm^{-3})	r (pc)	n (cm^{-3})
1	0.5	5.0E3	0.2	5.0E3	0.8	1.0E3	2.5	1.0E2	0.5	5.0E3
2	1.0	1.0E3	0.5	1.0E3	1.3	1.0E3	3.0	1.0E2	1.0	1.0E3
3	1.6	1.0E3	0.9	7.5E2	1.8	8.0E2	3.5	1.0E2	1.6	8.0E2
4	2.0	8.0E2	1.4	5.0E2	2.8	5.0E2	4.0	1.0E2	2.0	5.0E2
5	2.5	5.0E2	1.9	5.0E2	3.5	1.0E2	4.5	1.0E2	2.5	2.0E2
6	4.0	1.0E2	2.1	1.0E2	4.5	1.0E2	5.0	7.5E2	3.0	1.0E2
7	4.5	7.5E2	2.5	1.0E2	5.3	1.0E2	8.0	7.5E1	3.5	1.0E2
8	5.0	5.0E1	2.8	1.0E2	6.0	7.5E1	15	5.0E1	4.0	1.0E2
9	6.0	5.0E1	4.7	7.5E1	7.5	5.0E1	20	5.0E1	4.1	7.5E1
10	8.0	5.0E1	7.5	5.0E1	23	5.0E1	30	2.5E1	4.2	5.0E1
T (K)	1.25E3		1.0E4		1.2E4		1.0E4		1.25E4	
d (kpc)	6.5		7.5		6.0		6.0		6.0	
S_0 (s^{-1})	1.9E50		6.0E49		5.9E50		1.2E51		1.0E50	

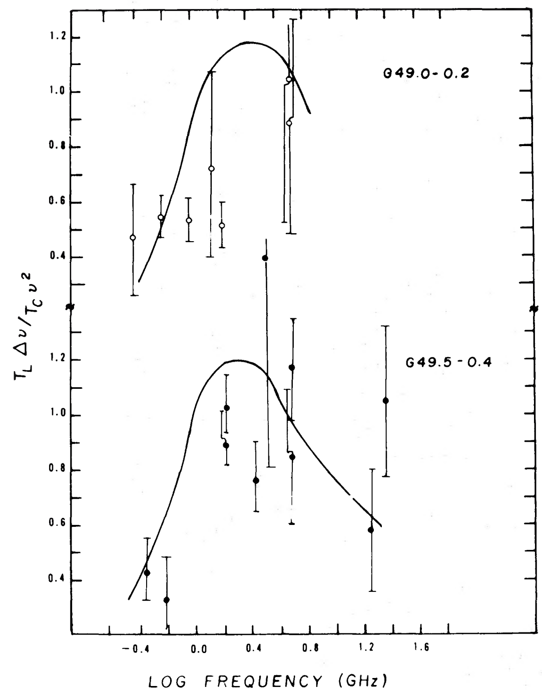

FIG. 12.—The line-to-continuum ratio predicted by models of the H II regions within the W51 complex (Table 3). The observed values (Table 1) are superposed onto the calculated curves.

In this expression the non–LTE line absorption coefficient for a recombination line from level N was written (Brocklehurst and Seaton 1972) $\kappa^L = b_N \beta_N \kappa^L(\mathrm{TE})$. The values for b_N and β_N were taken from Brocklehurst (1970), and the Voigt profile in $\kappa^L(\mathrm{TE})$ was evaulated according to the approximations in Landolt (1965).

Given the accuracy of the data, which at some frequencies are inconsistent within the quoted errors, the models seem to represent the observations reasonably well. Unlike the computations of the continuum flux density, the line-to-continuum ratio is very sensitive to the chosen kinetic temperature. The value given for the isothermal temperature in Table 3 is the one which best fits the line data. As in the models for the continuum, low-density ionized gas seems to be required for the low-frequency, high-N-number lines. High densities quench the high-N lines.

V. CONCLUSIONS

As in our previous study of W49 A, we have observed the different gaseous constituents of the H II region–molecular cloud complex W51. From the information obtained we were able to construct a picture of this active region of star formation in the Sagittarius spiral arm. From our models representing the ionized gas in this complex, we conclude that some of the H II regions are near the outside of the cold gas clouds.

We thank Dr. C. R. O'Dell of the Marshall Space Flight Center for his advice and encouragement during the early stages of this study.

REFERENCES

Altenhoff, W. J., Downes, D., Goad, L., Maxwell, A., and Rinehart, R. 1970, *Astr. Ap. Suppl.*, **1**, 319.
Bieging, J. 1975, in H II *Regions and Related Topics*, ed. T. L. Wilson and D. Downes (Heidelberg: Springer-Verlag), p. 443.
Brocklehurst, M. 1970, *M.N.R.A.S.*, **148**, 417.
Brocklehurst, M., and Seaton, M. J. 1972, *M.N.R.A.S.*, **157**, 179.
Burton, W. B. 1966, *Bull. Astr. Inst. Netherlands*, **18**, 247.
———. 1970*a*, *Astr. Ap. Suppl.*, **2**, 261.
———. 1970*b*, *Astr. Ap. Suppl.*, **2**, 291.
Burton, W. B., Gordon, M. Z., Bania, T. M., and Lockman, F. J. 1975, *Ap. J.*, **202**, 30.
Burton, W. B., and Liszt, H. S. 1979, in preparation.
Burton, W. B., and Shane, W. W. 1970, in *IAU Symposium No. 38, The Spiral Structure of Our Galaxy*, ed. W. Becker and G. Contopoulos (Dordrecht: Reidel), p. 397.
Chaisson, E. J. 1974, *A.J.*, **70**, 555.
Churchwell, E., and Edrich, J. 1970, *Astr. Ap.*, **6**, 261.
Crampton, D., Georgelin, Y. M., and Georgelin, Y. P. 1978, *Astr. Ap.*, **66**, 1.
Dieter, N. H. 1967, *Ap. J.*, **150**, 435.
Fomanlont, E., and Weliachew, G. 1973, *Ap. J.*, **181**, 781.
Gardner, F. F., and Morimoto, M. 1968, *Australian J. Phys.*, **21**, 881.
Goldsmith, P. F., Plambeck, R. L., and Chiao, R. Y. 1975, *Ap. J. (Letters)*, **196**, L39.
Gordon, K. J., Gordon, C. P., and Lockman, F. J. 1974, *Ap. J.*, **192**, 337.
Goss, W. M., and Shaver, P. A. 1970, *Australian J. Phys., Ap. Suppl.*, **14**, 1.
Gull, T. R., and Balick, B. 1974, *Ap. J.*, **192**, 63.
Hulse, R. A., and Taylor, J. H. 1974, *Ap. J. (Letters)*, **191**, L59.

Kraus, J. D. 1966, *Radio Astronomy* (New York: McGraw-Hill).
Kundu, M. R., and Velusamy, T. 1967, *Ann. Ap.*, **30**, 59.
Landolt, H. H. 1965, *Landolt-Börnstein: Numerical Data and Functional Relationships in Science and Technology*, n.s. Group 6, Vol. **1**, *Astronomy and Astrophysics* (Berlin: Springer-Verlag), p. 449.
Lin, C. C. 1971, in *Highlights of Astronomy*, Vol. **2**, ed. C. de Jager (Dordrecht: Reidel), p. 88.
Liszt, H. S. 1973, Ph.D. thesis.
Liszt, H. S., and Linke, R. A. 1975, *Ap. J.*, **196**, 709.
Lockman, F. J., and Brown, R. L. 1976, *Ap. J.*, **207**, 436.
MacLeod, J. M., and Doherty, L. H. 1968, *Ap. J.*, **154**, 833.
Martin, A. H. M. 1972, *M.N.R.A.S.*, **157**, 31.
McGee, R. X., and Gardner, F. F. 1968, *Australian J. Phys.*, **21**, 149.
Mezger, P. G., Schraml, J., and Terzian, Y. 1967, *Ap. J.*, **150**, 807.
Morgan, W. W., and Osterbrock, D. E. 1969, *A.J.*, **74**, 515.
Morris, M. 1976, *Ap. J.*, **210**, 100.
Mufson, S. L., and Liszt, H. S. 1977, *Ap. J.*, **212**, 664 (Paper I).
Palmer, P., Zuckerman, B., Penfield, H., Lilley, A. E., and Mezger, P. G. 1969, *Ap. J.*, **156**, 887.
Pankonin, V., Parrish, A., and Terzian, Y. 1974, *Astr. Ap.*, **37**, 411.
Papadopoulos, G. D., Lo, K. Y., Rosenkranz, P., and Chaisson, E. J. 1972, *Ap. Letters*, **10**, 89.
Parrish, A. 1972, *Ap. J.*, **174**, 33.
Pauliny-Toth, I. I. K., Wade, C. J., and Heeschen, D. S. 1966, *Ap. J. Suppl.*, **13**, 65.
Pedlar, A., and Davies, R. D. 1972, *M.N.R.A.S.*, **159**, 129.
Penzias, A. A., Jefferts, K. B., and Wilson, R. W. 1971, *Ap. J.*, **165**, 229.
Penzias, A. A., Solomon, P. M., Wilson, R. W., and Jefferts, K. B 1971, *Ap. J.* (*Letters*), **168**, L53.
Radhakrishnan, V., Goss, W. M., Murray, J. D., and Brooks, J. W. 1972, *Ap. J. Suppl.*, **24**, 49.
Reifenstein, E. C., Wilson, T. L., Burke, B. F., Mezger, P. G., and Altenhoff, W. J. 1970, *Astr. Ap.*, **4**, 357.
Roberts, W. W. 1969, *Ap. J.*, **158**, 123.
Schraml, J., and Mezger, P. G. 1969, *Ap. J.*, **156**, 269.
Scott, P. F. 1978, *M.N.R.A.S.*, **183**, 435.
Scoville, N. Z., and Solomon, P. M. 1973, *Ap. J.*, **180**, 31.
Shane, W. W., and Bieger-Smith, G. P. 1966, *Bull. Astr. Inst. Netherlands*, **18**, 263.
Shaver, P. A. 1969, *M.N.R.A.S.*, **142**, 273.
Slysh, V. I. 1974, *Soviet Astr.—AJ*, **18**, 278.
Snyder, L. E., and Buhl, D. 1971, *Ap. J.* (*Letters*), **163**, L47.
Terzian, Y., and Balick, B. 1969, *A.J.*, **74**, 76.
Turner, B. E., Zuckerman, B., Palmer, P., and Morris, M. 1973, *Ap. J.*, **186**, 123.
Ulich, B. L., and Haas, R. W. 1976, *Ap. J. Suppl.*, **30**, 247.
Waltman, W. B., and Johnston, K. J. 1973, *Ap. J.*, **182**, 489.
Weaver, H., Dieter, N. H., and Williams, D. R. W. 1968, *Ap. J. Suppl.*, **16**, 219.
Wendker, H., and Yang, K. S. 1968, *A.J.*, **73**, 61.
Westerhout, G. 1958, *Bull. Astr. Inst. Netherlands*, **14**, 215.
Wilson, T. L., Bieging, J., Downes, D., and Gardner, F. F. 1976, *Astr. Ap.*, **51**, 303.
Wilson, T. L., Mezger, P. G., Gardner, F. F., and Milne, D. K. 1970, *Ap. Letters*, **5**, 99.
Woodward, P. R. 1975, *Ap. J.*, **195**, 61.
Wynn-Williams, C. G., Becklin, E. E., and Neugebauer, G. 1974, *Ap. J.*, **187**, 473.
Zuckerman, B., Buhl, D., Palmer, P., and Snyder, L. E. 1970, *Ap. J.*, **160**, 485.
Zuckerman, B., and Palmer, P. 1970, *Astr. Ap.*, **4**, 244.

HARVEY S. LISZT: National Radio Astronomy Observatory, Edgemont Road, Charlottesville, VA 22901
STUART L. MUFSON: Astronomy Department, Indiana University, Bloomington, IN 47401